ChemComm

Chemical Communications

rsc.li/chemcomm

ROYAL SOCIETY
OF CHEMISTRY
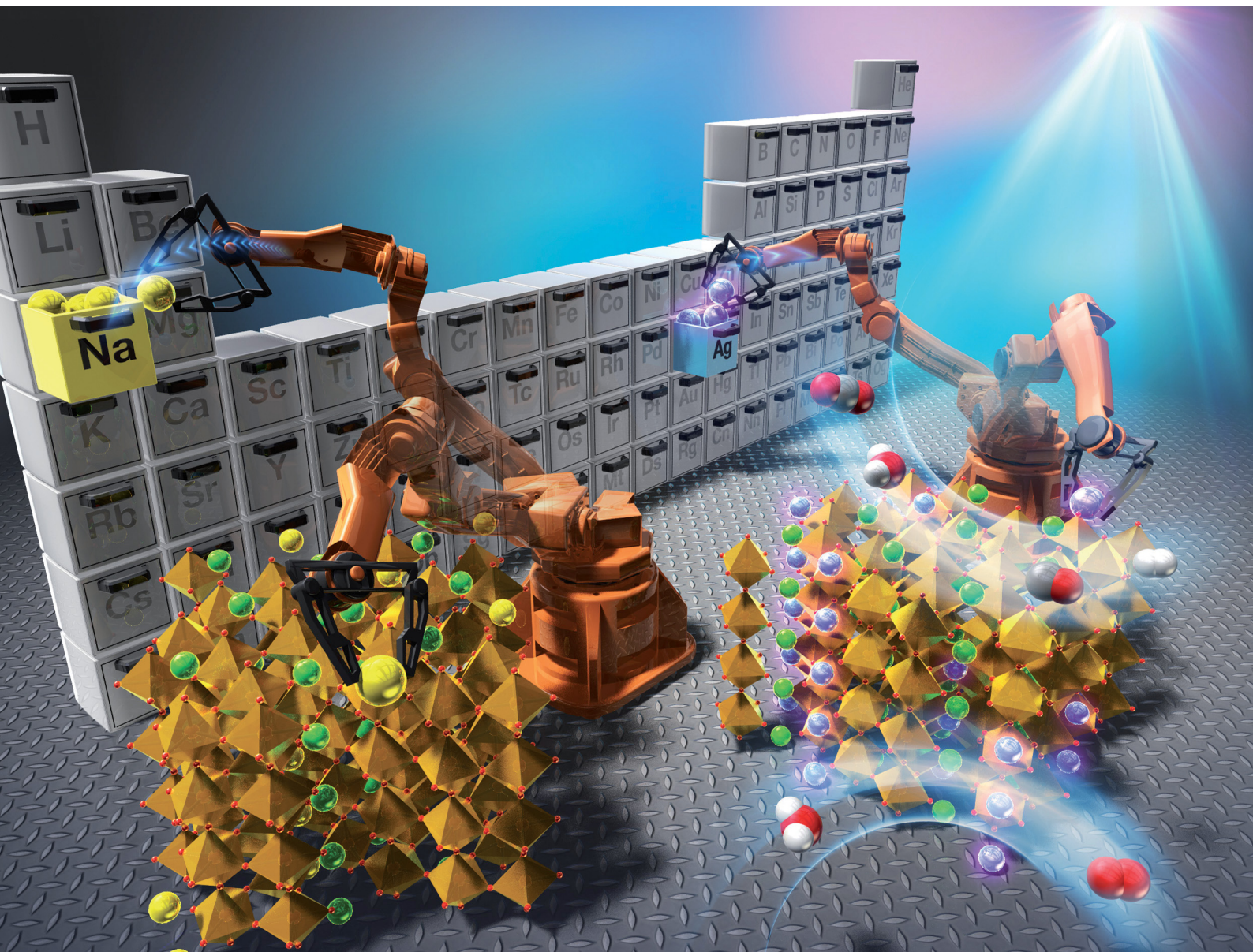
COMMUNICATION
Akihiko Kudo *et al.*
Water splitting and CO_2 reduction over an $AgSr_2Ta_5O_{15}$
photocatalyst developed by a valence band control strategy

Check for updates

Water splitting and CO_2 reduction over an $AgSr_2Ta_5O_{15}$ photocatalyst developed by a valence band control strategy†

Tomoaki Takayama, ‡[a] Akihide Iwase §[a] and Akihiko Kudo ⋆[ab]

Ag^+ substitution was applied to a tungsten-bronze-type metal oxide. An $AgSr_2Ta_5O_{15}$ photocatalyst has emerged for water splitting and CO_2 reduction. DFT calculation and diffuse reflection spectra revealed that the Ag d-orbital formed a new valence band, leading to a narrow band gap (3.91 eV) compared to that of $NaSr_2Ta_5O_{15}$ (4.11 eV).

Photocatalytic water splitting and CO_2 reduction using water as an electron donor are attractive from the viewpoint of artificial photosynthesis.[1,2] Metal oxides have been widely studied as photocatalysts.[1] This is because most metal oxides are stable under photocatalytic reaction conditions. However, these metal oxide photocatalysts generally possess wide band gaps, resulting in limitation of their responses to irradiation lights with shorter wavelengths. In this context, many efforts have been made to narrow their band gaps.

Band engineering,[3] including valence band control, doping, and solid solution formation, is an effective strategy for narrowing the band gap. Among them, the valence band control technique has indeed developed metal oxide photocatalysts with narrower band gaps. In this strategy, $Cu^+(3d^{10})$,[4–9] $Ag^+(4d^{10})$,[10–16] $Sn^{2+}(5s^2)$,[17–20] $Pb^{2+}(6s^2)$,[13,21] and $Bi^{3+}(6s^2)$[13,22–25] make new valence bands at shallower levels than O2p-based valence bands. Among the photocatalysts developed by this strategy, $AgTaO_3$[10] and $Na_{0.5}Bi_{0.5}TiO_3$[24] photocatalysts with perovskite structures efficiently split water to H_2 and O_2 in stoichiometric amounts. However, the numbers of valence-band-controlled metal oxide photocatalysts for water splitting in a one-photon excitation mechanism are still limited to mainly the typical perovskites, resulting in a few crystal structures being useful for the valence band control strategy.

A tungsten-bronze-type crystal structure is one of the families of perovskite materials which are generally denoted as the chemical formula ABO_3. A notable feature in the crystal structure of tungsten bronze is that it is easy to replace A and A′ site cations of its chemical formula $(AA'_2M_5O_{15})$ with various cations. For example, the A site can contain Na^+ and K^+ cations, and the A′ sites can contain Ca^{2+}, Sr^{2+}, and Ba^{2+} cations, whereas the M sites can contain Nb^{5+} and Ta^{5+} cations. To date, it has been reported that $KCaSrTa_5O_{15}$[26,27] and $KSr_2Ta_5O_{15}$[28] show photocatalytic activities for water splitting and CO_2 reduction using water as an electron donor. A series of $AA'_2Ta_5O_{15}$ (A = K, Na; A′ = Sr, Ba)[29,30] and $K_2RETa_5O_{15}$ (RE = rare earth metal)[31] are also tungsten-bronze-type photocatalysts. Therefore, these materials are expected to contribute to expanding the crystal structures for a valence band controlled photocatalyst.

In this study, we successfully prepared $AgSr_2Ta_5O_{15}$ with a tungsten-bronze-type structure and compared its band structure to that of $NaSr_2Ta_5O_{15}$ based on diffuse reflectance spectra and density functional theory (DFT) calculation. Moreover, the photocatalytic property of $AgSr_2Ta_5O_{15}$ for water splitting and CO_2 reduction was evaluated.

$NaSr_2Ta_5O_{15}$ was prepared by a polymerized complex method (PC method) that usually gives high photocatalytic performances compared with a conventional solid-state reaction.[27] $AgSr_2Ta_5O_{15}$ was prepared by a solid-state reaction because it would not be easy to prepare it by the PC method due to the isolation of metallic Ag. The obtained $AgSr_2Ta_5O_{15}$ was treated with an aqueous HNO_3 solution, if necessary. Their crystal phases were identified by X-ray diffraction. Their diffuse reflectance spectra were obtained using the Kubelka–Munk method. Particle shapes of $AgSr_2Ta_5O_{15}$ and $NaSr_2Ta_5O_{15}$ were observed using a scanning electron microscope. Photocatalytic CO_2 reduction and water splitting were conducted

[a] *Department of Applied Chemistry, Faculty of Science, Tokyo University of Science, 1-3 Kagurazaka, Shinjuku-ku, Tokyo 162-8601, Japan. E-mail: a-kudo@rs.tus.ac.jp*

[b] *Tokyo University of Science, Research Institute of Science and Technology, Carbon Value Research Center, Japan*

‡ Present address: His current affiliation is Graduate School of Science and Technology, Division of Materials Science, Nara Institute of Science and Technology, 8916-5 Takayama, Ikoma, Nara 630-0192, Japan.

§ Present address: His current affiliation is Department of Applied Chemistry, School of Science and Technology, Meiji University, Kanagawa 214-8571, Japan.
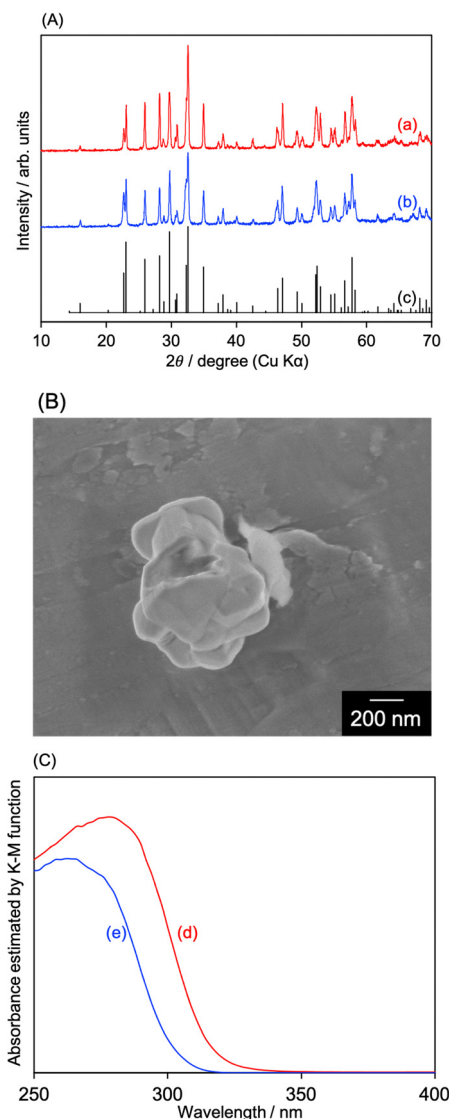
Fig. 1 (A) XRD patterns of (a) $AgSr_2Ta_5O_{15}$ (w/o HNO_3) and (b) $NaSr_2Ta_5O_{15}$, and PDF of (c) $NaSr_2Ta_5O_{15}$ (PDF No.: 39-1439). (B) SEM image of $AgSr_2Ta_5O_{15}$ (w/o HNO_3). (C) DRS of (d) $AgSr_2Ta_5O_{15}$ (w/o HNO_3) and (e) $NaSr_2Ta_5O_{15}$.

using a gas-flow system equipped with inner irradiation cells made of quartz and Pyrex, and a 400 W high-pressure mercury lamp. Density functional theory (DFT) calculations were performed using the CASTEP code to obtain band structures of $AgSr_2Ta_5O_{15}$ and $NaSr_2Ta_5O_{15}$. The detailed information of these experiments is summarized in the supporting information (including Fig. S1–S3 and Table S1, ESI†).

Fig. 1(A) shows X-ray diffraction patterns (XRDs) of $AgSr_2Ta_5O_{15}$ (not treated with an aqueous HNO_3 solution; denoted with "w/o HNO_3") and $NaSr_2Ta_5O_{15}$. The diffraction peaks of both samples were well consistent with those of a powder diffraction file (PDF) of $NaSr_2Ta_5O_{15}$. This is because of the resembled ionic radii of Ag^+ (115 pm) and Na^+ (102 pm) in the 6 coordination number. For $AgSr_2Ta_5O_{15}$ (w/o HNO_3), $AgTaO_3$ and metallic Ag were not observed in the XRD pattern

(Fig. S4, ESI†). Scanning electron microscopy (SEM) was performed to observe $AgSr_2Ta_5O_{15}$ and $NaSr_2Ta_5O_{15}$ particles (Fig. 1(B) and Fig. S5, ESI†). Sintered particles with a size of several hundred nm were observed. Diffuse reflectance spectra (DRS) of $AgSr_2Ta_5O_{15}$ and $NaSr_2Ta_5O$ are shown in Fig. 1(C). The absorption spectrum red-shifted by replacing Na^+ with Ag^+, resulting in their band gaps of 3.91 eV for $AgSr_2Ta_5O_{15}$ and 4.11 eV for $NaSr_2Ta_5O_{15}$. The reason why the band gap was narrowed by containing Ag^+ is due to a new valence band formed by the hybridization of O2p and Ag4d orbitals. These physico-chemical analyses indicate that $AgSr_2Ta_5O_{15}$ of a tungsten-bronze-type crystal structure was successfully formed, and that its band gap was narrowed by Ag^+ substitution as seen for $NaTaO_3$ and $AgTaO_3$.[10] Density functional theory (DFT) calculation was performed to discuss the band structures of $AgSr_2Ta_5O_{15}$ and $NaSr_2Ta_5O_{15}$, as shown in Fig. 2. Conduction band minima of both samples were mainly formed by Ta d-orbital and O p-orbital, whereas both valence band maxima contained O p-orbital. Most importantly, the Ag d-orbital took part in making the valence band of $AgSr_2Ta_5O_{15}$, whereas the Na s-orbital did not make such a valence band. This is well consistent with the band structure of the $AgTaO_3$ photocatalyst.[10] Thus, Ag^+ substitution is effective to narrow the band gap of the tungsten-bronze-type metal oxide by forming the new valence band. The calculated band gaps of $AgSr_2Ta_5O_{15}$ and $NaSr_2Ta_5O_{15}$ were 3.25 and 3.28 eV, respectively. These values are
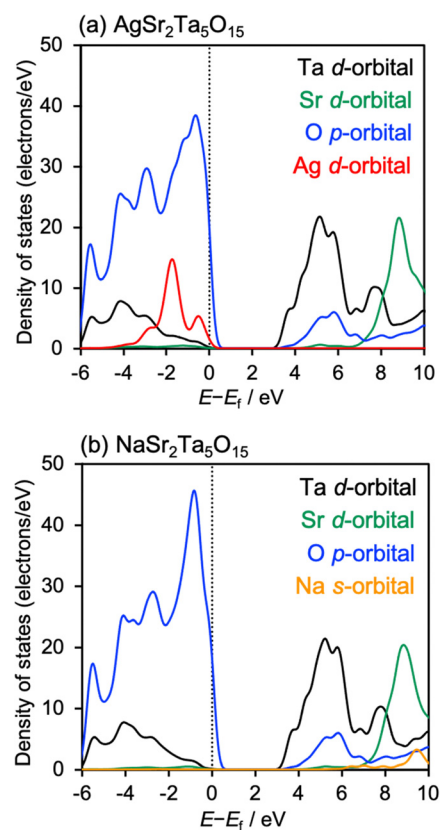

Fig. 2 DOS of (a) $AgSr_2Ta_5O_{15}$ and (b) $NaSr_2Ta_5O_{15}$. The dotted lines indicate their Fermi levels.

small as compared to those experimentally obtained from DRS, even though HSE06 was used. This might be due to deviation of the optimized structures in the DFT calculation from the experimentally obtained samples; *e.g.*, structural isomerism (Fig. S1 and S2, ESI†).[32–34]

Photocatalytic performances of $AgSr_2Ta_5O_{15}$ and $NaSr_2Ta_5O_{15}$ were evaluated, as shown in Table 1. $NaSr_2Ta_5O_{15}$ with NiO and Ag cocatalysts showed higher photocatalytic activities for water splitting and CO_2 reduction than $AgSr_2Ta_5O_{15}$ (entries 1, 2, 5, 7). This is probably due to the enhancement of recombination between photogenerated e^- and h^+ at a silver site, more or less. Next, let us see $AgSr_2Ta_5O_{15}$ newly obtained in the present study.

Bare $AgSr_2Ta_5O_{15}$ split water into H_2 and O_2 (entry 3). Its performance was improved by loading NiO, which is a typical cocatalyst for water splitting (entry 4).[3] Considering the literature about $AgTaO_3$,[10] there is a possibility that Ag nanoparticles are segregated on the surface. Therefore, $AgSr_2Ta_5O_{15}$ was treated with an aqueous HNO_3 solution to remove the Ag nanoparticles, resulting in an improvement in the water splitting performance (entry 5). The treated $AgSr_2Ta_5O_{15}$ photocatalyst was applied to CO_2 reduction using water as an electron donor (entries 6–9). We have reported that an Ag cocatalyst loaded by impregnation works as an active site for CO_2 reduction to form CO.[2,35–37] The Ag-impregnated $AgSr_2Ta_5O_{15}$ produced not only H_2 and O_2 but also CO under CO_2 gas conditions. Because bare $AgSr_2Ta_5O_{15}$ did not give CO under Ar (entry 3), we can conclude that the evolved CO was generated from not contamination of carbonous species over the photocatalyst but CO_2. When the amount of Ag cocatalyst was increased, the CO formation rate and its selectivity were improved. The addition of $NaHCO_3$ was effective for CO_2 reduction.

Fig. 3 shows photocatalytic CO_2 reduction over Ag(3 wt%)-loaded $AgSr_2Ta_5O_{15}$ (Table 1 entries 8, 9). H_2, CO, and O_2 were formed from water dissolved with CO_2 gas (1 atm). The activity was improved by adding $NaHCO_3$. It is reported that the hydrogen carbonate enhances O_2 production in water splitting over a Pt/TiO_2 photocatalyst.[38] The selectivity for CO formation (Sel_{CO}) was also drastically improved up to 77%. This is because
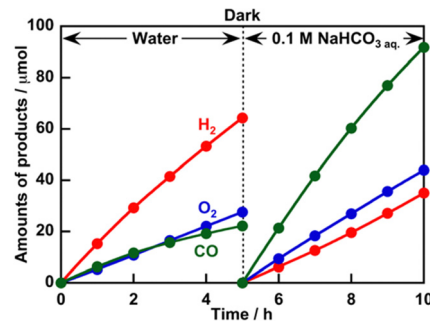

Fig. 3 CO_2 reduction using water as an electron donor over the Ag (3 wt%)-loaded $AgSr_2Ta_5O_{15}$ photocatalyst. Photocatalyst: 0.5 g, Reactant solution: water (350 mL), Reactor: a gas-flow system with an inner irradiation cell made of quartz, Light source: a 400 W high-pressure mercury lamp, Concentration of the aqueous $NaHCO_3$ solution: 0.1 mol L^{-1}.

of the smooth supply of CO_2 molecules onto the active site due to a chemical equilibrium of the hydrogen carbonate.[2,36] The ratios of H_2/O_2 and $(H_2 + CO)/O_2$ were slightly beyond stoichiometry (*i.e.*, beyond two). According to the literature about $AgTaO_3$,[10] a part of the evolved O_2 might be adsorbed on the $AgTaO_3$ photocatalyst, resulting in the O_2 evolution being slightly less than the stoichiometry in an early period for water splitting. For the present CO_2 reduction over $Ag/AgSr_2Ta_5O_{15}$, the rates of gas evolution became gradually close to stoichiometry with the reaction time (Fig. S6, ESI†). Therefore, there is a possibility that the evolved O_2 was partly adsorbed on $AgSr_2Ta_5O_{15}$.

Fig. 4 shows the effect of the wavelength of the irradiation light on photocatalytic CO_2 reduction over $AgSr_2Ta_5O_{15}$ without HNO_3 treatment (w/o HNO_3). $AgSr_2Ta_5O_{15}$ (w/o HNO_3) was active for CO_2 reduction even without additional Ag cocatalyst loading (1st run). The CO formation rate and its selectivity were improved by adding $NaHCO_3$ (2nd run). This result implies that a small amount of Ag nanoparticles would be segregated on the surface of $AgSr_2Ta_5O_{15}$ prepared by a solid-state reaction as seen in $AgTaO_3$, though it was not detected by XRD and DRS. The segregated Ag worked as the active site for CO_2 reduction. Additionally, it is noteworthy that the $AgSr_2Ta_5O_{15}$ (w/o HNO_3)

Table 1 Photocatalytic water splitting and CO_2 reduction over $AgSr_2Ta_5O_{15}$

Entry	Photocatalyst	HNO_3 treatment	Cocatalyst (wt%)	Gas	$NaHCO_3$ addition	Activity/µmol h^{-1} H_2	O_2	CO	Sel_{CO} %
1	$NaSr_2Ta_5O_{15}$	No	NiO(0.2)	Ar	No	1365	714	—	—
2	$NaSr_2Ta_5O_{15}$	No	Ag(0.5)	CO_2	Yes	25	29	29	54
3	$AgSr_2Ta_5O_{15}$	No	—	Ar	No	80	34	0	0
4	$AgSr_2Ta_5O_{15}$	No	NiO(0.2)	Ar	No	197	76	—	—
5	$AgSr_2Ta_5O_{15}$	Yes	NiO(0.2)	Ar	No	457	204	—	—
6	$AgSr_2Ta_5O_{15}$	Yes	Ag(0.5)	CO_2	No	25	11	2.5	9.1
7	$AgSr_2Ta_5O_{15}$	Yes	Ag(0.5)	CO_2	Yes	17	12	13	43
8	$AgSr_2Ta_5O_{15}$	Yes	Ag(3)	CO_2	No	15	5.2	6.2	29
9	$AgSr_2Ta_5O_{15}$	Yes	Ag(3)	CO_2	Yes	6.2	9.3	21	77

Photocatalyst: 0.5 g, Reactant solution: water (350 mL), Reactor: a gas-flow system with an inner irradiation cell made of quartz, Light source: a 400 W high-pressure mercury lamp, Concentration of the aqueous $NaHCO_3$ solution: 0.1 mol L^{-1}. Selectivity of CO formation (Sel_{CO}) was estimated as follows; Sel_{CO} (%) = (the CO formation rate)/[(the H_2 formation rate) + (the CO formation rate)] × 100.

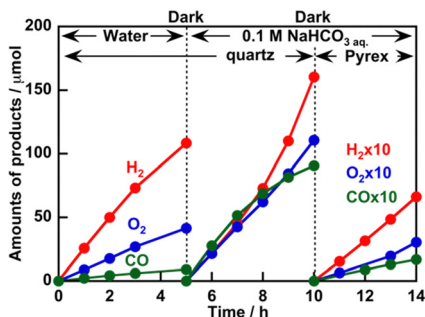**Fig. 4** CO_2 reduction using water as an electron donor over the $AgSr_2Ta_5O_{15}$ (w/o HNO_3) photocatalyst without any additional cocatalyst loading. Photocatalyst: 0.5 g, Reactant solution: water (350 mL), Reactor: a gas-flow system with an inner irradiation cell made from quartz ($\lambda > 250$ nm) or Pyrex ($\lambda > 300$ nm), Light source: a 400 W high-pressure mercury lamp, Concentration of an aqueous $NaHCO_3$ solution: 0.1 mol L^{-1}.

produced H_2, CO, and O_2 under irradiation of light with wavelength longer than 300 nm. This is a feature of the $AgSr_2Ta_5O_{15}$ possessing a red-shifted absorption edge as shown in Fig. 1(C) being different from $NaSr_2Ta_5O_{15}$. $AgSr_2Ta_5O_{15}$ is superior to $NaSr_2Ta_5O_{15}$ in this photoresponse. Thus, $AgSr_2Ta_5O_{15}$ (w/o HNO_3) is a photocatalyst that is active not only for water splitting but also for CO_2 reduction using water as an electron donor.

In conclusion, $AgSr_2Ta_5O_{15}$ was prepared by a conventional solid-state reaction based on a valence band control strategy using Ag^+ substitution. Its crystal structure was almost the same as that of $NaSr_2Ta_5O_{15}$ due to the resembled ionic radii of Ag^+ and Na^+. This Ag^+ substitution resulted in red-shift of the absorption spectrum from that of $NaSr_2Ta_5O_{15}$. The band gap of $AgSr_2Ta_5O_{15}$ was 3.91 eV, while that of $NaSr_2Ta_5O_{15}$ was 4.11 eV. DOS estimated by DFT calculations revealed that the Ag d-orbital took part in making the new valence band. Furthermore, $AgSr_2Ta_5O_{15}$ was a new photocatalyst for water splitting and CO_2 reduction. This study demonstrated the usefulness of the valence band control strategy for the development of new metal oxide photocatalysts, resulting in the $AgSr_2Ta_5O_{15}$ photocatalyst with a tungsten-bronze type crystal structure. This finding will contribute to liberating the valence band control strategy from the material design space mainly limited in typical perovskite-type metal oxides for the development of active photocatalysts for water splitting and CO_2 reduction.

Conflicts of interest

There are no conflicts to declare.

Notes and references

1 Q. Wang and K. Domen, *Chem. Rev.*, 2020, **120**, 919.
2 S. Yoshino, T. Takayama, Y. Yamaguchi, A. Iwase and A. Kudo, *Acc. Chem. Res.*, 2022, **55**, 966.
3 A. Kudo and Y. Miseki, *Chem. Soc. Rev.*, 2009, **38**, 253.
4 H. Kato, A. Takeda, M. Kobayashi, M. Hara and M. Kakihana, *Catal. Sci. Technol.*, 2013, **3**, 3147.
5 K. Iwashina, A. Iwase and A. Kudo, *Chem. Sci.*, 2015, **6**, 687.
6 H. Kato, T. Fujisawa, M. Kobayashi and M. Kakihana, *Chem. Lett.*, 2015, **44**, 973–975.
7 K. Iwashina, A. Iwase, S. Nozawa, S. Adachi and A. Kudo, *Chem. Mater.*, 2016, **28**, 4677.
8 I. Sullivan, B. Zoellner and P. A. Maggard, *Chem. Mater.*, 2016, **28**, 5999.
9 B. Zoellner, S. Stuart, C.-C. Chung, D. B. Dougherty, J. Jones and P. A. Maggard, *J. Mater. Chem. A*, 2016, **4**, 3115.
10 H. Kato, H. Kobayashi and A. Kudo, *J. Phys. Chem. B*, 2002, **106**, 12441.
11 Y. Hosogi, H. Kato and A. Kudo, *J. Mater. Chem.*, 2008, **18**, 647.
12 J. Boltersdorf and P. A. Maggard, *ACS Catal.*, 2013, **3**, 2547.
13 J. Boltersdorf, T. Wong and P. A. Maggard, *ACS Catal.*, 2013, **3**, 2943.
14 H. Horie, A. Iwase and A. Kudo, *ACS Appl. Mater. Interfaces*, 2015, **7**, 14638.
15 S. Zong, C. Cheng, J. Shi, Z. Huang, Y. Hu, H. Yang and L. Guo, *Chem. – Asian J.*, 2017, **12**, 882.
16 K. Watanabe, A. Iwase, S. Nozawa, S. Adachi and A. Kudo, *ACS Sustainable Chem. Eng.*, 2019, **7**, 9881.
17 Y. Hosogi, H. Kato and A. Kudo, *J. Phys. Chem. C*, 2008, **112**, 17678.
18 Y. Hosogi, Y. Shimodaira, H. Kato, H. Kobayashi and A. Kudo, *Chem. Mater.*, 2008, **20**, 1299.
19 J. Boltersdorf, I. Sullivan, T. L. Shelton, Z. Wu, M. Gray, B. Zoellner, F. E. Osterloh and P. A. Maggard, *Chem. Mater.*, 2016, **28**, 8876.
20 D. Noureldine and K. Takanabe, *Catal. Sci. Technol.*, 2016, **6**, 7656.
21 Y. Shimodaira, H. Kato, H. Kobayashi and A. Kudo, *Bull. Chem. Soc. Jpn.*, 2007, **80**, 885.
22 A. Kudo, K. Omori and H. Kato, *J. Am. Chem. Soc.*, 1999, **121**, 11459.
23 H. Fujito, H. Kunioku, D. Kato, H. Suzuki, M. Higashi, H. Kageyama and R. Abe, *J. Am. Chem. Soc.*, 2016, **138**, 2082.
24 K. Watanabe, Y. Iikubo, Y. Yamaguchi and A. Kudo, *Chem. Commun.*, 2021, **57**, 323.
25 D. Ozaki, H. Suzuki, O. Tomita, Y. Inaguma, K. Nakashima, H. Kageyama and R. Abe, *J. Photochem. Photobiol., A*, 2021, **408**, 113095.
26 T. Takayama, K. Tanabe, K. Saito, A. Iwase and A. Kudo, *Phys. Chem. Chem. Phys.*, 2014, **16**, 24417.
27 T. Takayama, A. Iwase and A. Kudo, *Bull. Chem. Soc. Jpn.*, 2015, **88**, 538.
28 Z. Huang, K. Teramura, S. Hosokawa and T. Tanaka, *Appl. Catal., B*, 2016, **199**, 272.
29 Z. Huang, S. Yoshizawa, K. Teramura, H. Asakura, S. Hosokawa and T. Tanaka, *ACS Omega*, 2017, **2**, 8187.
30 Z. Huang, S. Yoshizawa, K. Teramura, H. Asakura, S. Hosokawa and T. Tanaka, *ACS Sustainable Chem. Eng.*, 2018, **6**, 8247.
31 Z. Huang, K. Teramura, H. Asakura, S. Hosokawa and T. Tanaka, *Catal. Today*, 2018, **300**, 173.
32 A. Kubo, G. Giorgi and K. Yamashita, *J. Phys. Chem. C*, 2017, **121**, 27813.
33 A. Kubo, G. Giorgi and K. Yamashita, *Chem. Mater.*, 2017, **29**, 539.
34 M. Kaneko, M. Fujii, T. Hisatomi, K. Yamashita and K. Domen, *J. Energy Chem.*, 2019, **36**, 7.
35 K. Iizuka, T. Wato, Y. Miseki, K. Saito and A. Kudo, *J. Am. Chem. Soc.*, 2011, **133**, 20863.
36 H. Nakanishi, K. Iizuka, T. Takayama, A. Iwase and A. Kudo, *ChemSusChem*, 2017, **10**, 112.
37 T. Takayama, H. Nakanishi, M. Matsui, A. Iwase and A. Kudo, *J. Photochem. Photobiol., A*, 2018, **358**, 416.
38 K. Sayama and H. Arakawa, *J. Chem. Soc., Faraday Trans.*, 1997, **93**, 1647.